applied sciences

MDPI

Article

Atomic Layer Deposition TiO_2 Films and TiO_2/SiN_x Stacks Applied for Silicon Solar Cells

Zu-Po Yang [1], Hsyi-En Cheng [2], I-Hsuan Chang [2] and Ing-Song Yu [3,*]

[1] Institute of Photonic System, National Chiao Tung University, Tainan 71150, Taiwan; zupoyang@nctu.edu.tw
[2] Department of Electro-Optical Engineering, Southern Taiwan University of Science and Technology, Tainan 710, Taiwan; sean@mail.stust.edu.tw (H.-E.C.); ma0L0222@stust.edu.tw (I.-H.C.)
[3] Department of Materials Science and Engineering, National Dong Hwa University, Hualien 97401, Taiwan
* Correspondence: isyu@mail.ndhu.edu.tw; Tel.: +886-3-863-4219

Academic Editor: Paolo Minzioni
Received: 19 June 2016; Accepted: 12 August 2016; Published: 19 August 2016

Abstract: Titanium oxide (TiO_2) films and TiO_2/SiN_x stacks have potential in surface passivation, anti-reflection coatings and carrier-selective contact layers for crystalline Si solar cells. A Si wafer, deposited with 8-nm-thick TiO_2 film by atomic layer deposition, has a surface recombination velocity as low as 14.93 cm/s at the injection level of 1.0×10^{15} cm^{-3}. However, the performance of silicon surface passivation of the deposited TiO_2 film declines as its thickness increases, probably because of the stress effects, phase transformation, atomic hydrogen and thermal stability of amorphous TiO_2 films. For the characterization of 66-nm-thick TiO_2 film, the results of transmission electron microscopy show that the anatase TiO_2 crystallinity forms close to the surface of the Si. Secondary ion mass spectrometry shows the atomic hydrogen at the interface of TiO_2 and Si which serves for chemical passivation. The crystal size of anatase TiO_2 and the homogeneity of TiO_2 film can be deduced by the measurements of Raman spectroscopy and spectroscopic ellipsometry, respectively. For the passivating contacts of solar cells, in addition, a stack composed of 8-nm-thick TiO_2 film and a plasma-enhanced chemical-vapor-deposited 72-nm-thick SiN_x layer has been investigated. From the results of the measurement of the reflectivity and effective carrier lifetime, TiO_2/SiN_x stacks on Si wafers perform with low reflectivity and some degree of surface passivation for the Si wafer.

Keywords: titanium oxide; atomic layer deposition; anatase; surface passivation; antireflection coating; carrier selective contact; silicon solar cell

1. Introduction

Dielectric thin-film materials capped on top of solar cells serve important roles as an anti-reflection coating layer for photon harvesting, and as a surface passivation layer to reduce the surface recombination loss for crystalline silicon (c-Si) solar cells. As the thickness of c-Si solar cells decreases due to lowering the manufacturing cost of solar cells, Si surface passivation becomes a more and more important issue for high efficiency solar cells [1]. Therefore, a variety of dielectric materials have been proposed for the surface passivation of solar cells, such as silicon dioxide (SiO_2), amorphous silicon nitride (a-SiN_x), amorphous silicon (a-Si), and aluminum oxide (Al_2O_3) [2–4]. Beside the use of dielectric thin films, Si surface passivation also depends on the deposition techniques, treatments of surface cleaning, and types of Si substrates. Among different deposition techniques, atomic layer deposition (ALD) shows highly conformal coating and extreme uniformity which is suitable for complex surface texturing and large-size industrial solar cells. For example, Al_2O_3 thin films deposited by ALD have shown great performance in surface passivation for industrial c-Si solar cells [5–7]. In addition, the spatial ALD technique has demonstrated high-throughput fabrication for c-Si solar cells in the industry [8]. ALD bilayer coatings not only can provide a function for surface

passivation, but also can serve as anti-reflection coating layers to lower the reflectivity of solar cells, such as Al_2O_3/TiO_2, Al_2O_3/ZnS, Al_2O_3/HfO_2 and Al_2O_3/SiN_x stacks [9–11]. Recently, the concept of passivating contact was proposed to further increase the conversion efficiency of c-Si solar cells by using these dielectric materials. Carrier selection and integration of tunneling contacts have been developed to reduce the recombination losses between the photoactive part of the solar cell and the metal contacts. The ultrathin dielectric layers for conductive silicon surface passivation layers can be fabricated easily by the ALD technique [12–14].

Titanium oxide (TiO_2) film has been used in the photovoltaic industry as an anti-reflection coating since the 1980s due to its low growth temperature, nontoxic liquid precursors, excellent chemical resistance, optimal reflective index, and low absorbance at wavelengths of the solar spectrum (except the ultraviolet region) [15,16]. However, stoichiometric TiO_2 films afford little surface passivation on bare silicon wafer [17]. Doeswijk et al. reported that nonstoichiometric titanium oxide films deposited by pulsed laser deposition had a certain degree of passivation for the non-diffused *p*-type Si surface [18]. Thomson et al. proposed that the TiO_2 thin films deposited by atmospheric pressure chemical vapor deposition (APCVD) could effectively passivate *n*-type Si and boron-diffused surfaces. These films were also annealed at 300 °C in nitrogen (N_2) ambient and subjected to light soaking by a halogen lamp to create negative charges for further improving the performance of surface passivation [19,20]. Si surface passivation by TiO_2 thin films using the ALD technique was first reported in 2013 by Yu et al. [21]. In the study, 66-nm-thick TiO_2 films were deposited by ALD on the float-zone (FZ) Si wafers at different substrate temperatures (200 °C, 300 °C, 400 °C and 500 °C). The results showed that a certain degree of Si surface passivation was observed for relatively lower deposition temperature of TiO_2 films. Recently, Liao et al. reported excellent c-Si surface passivation by atomic layer–deposited amorphous TiO_2 films at even lower temperature (100 °C) and realized ultralow effective surface recombination velocities down to 2.8 cm/s and 8.3 cm/s for *n*-type and *p*-type FZ c-Si wafers, respectively [22]. They also demonstrated the excellent performance of passivation for the TiO_2 films on boron-doped industrial Si emitters, which further proved the feasibility of applying TiO_2 film in surface passivation for high efficiency *n*-type Si solar cells in the future [23]. In addition, Avasthi et al. reported that the TiO_2/Si heterojunction structure can selectively block the transport of holes from Si to the TiO_2 layer [24]. Yang et al. proposed ultrathin amorphous TiO_2 film as the carrier-selective contact layer in *n*-type Si solar cells and demonstrated the high conversion efficiency of Si solar cells with a simplified process [25,26].

Although many research groups demonstrated that TiO_2 films by ALD perform good surface passivation for Si solar cells [27], the characterization of those TiO_2 films is rarely reported in order to understand the mechanisms of Si surface passivation of TiO_2 films (chemical passivation and field-effect passivation). In this study, we investigated the growth and phase transformation of TiO_2 films deposited by ALD at the temperature of 200 °C by using transmission electron microscopy (TEM). The chemical compositions of TiO_2 films, especially for atomic hydrogen, were studied by secondary ion mass spectrometry (SIMS). The crystallinity of TiO_2 films was checked by Raman spectroscopy. The optical properties of these TiO_2 films were conducted by spectroscopic ellipsometry. Then, silicon surface passivation for TiO_2 thin films with different thicknesses and post-deposition annealing was performed. Finally, we studied the surface passivation and reflectivity of TiO_2/SiN_x stacks on Si wafers.

2. Materials and Methods

In the experiment, we used double-side polished FZ *p*-type Si wafers (Institute of Electronic Materials Technology, Warsaw, Poland) with the resistivity of 5000 Ω-cm, thickness of 275 μm, and orientation of (100). Before TiO_2 deposition, Si wafers were cleaned in sequence by acetone to remove the organics and by 5% hydrofluoric acid to remove the native oxide. Then, wafers were rinsed in deionized water and dried with N_2 gas. Right after the cleaning, Si substrate was placed in the reaction chamber and then the chamber temperature was raised to 200 °C for the ALD deposition [28].

For the process, we employed $TiCl_4$ and H_2O as the reactants and Ar (99.999%) as the purging gas. One cycle (one monolayer) of TiO_2 growth was 0.066 nm in thick and included eight steps, i.e., $TiCl_4$ reactant, pump-down, Ar purge, pump-down, H_2O reactant, pump-down, Ar purge, and pump-down. Due to the self-limiting growth of ALD, we grew four different thicknesses of TiO_2 thin films by controlling the cycle numbers (125, 250, 530, and 1000 cycles).

For the characterization of TiO_2 thin films, we used the Tecnai G2 TEM (FEI Company, Hillsboro, OR, USA) to study the crystallinity, phases and thickness of TiO_2. The samples for TEM were prepared by Dual Beam-Focused Ion Beam system. SIMS of Cameca IMS 6F (AMETEK S.A.S., Elancourt, France) was used to analyze the depth profiles of oxygen, silicon and hydrogen. Jobin Yvon U1000 Raman spectroscopy (HORIBA, Kyoto, Japan) equipped a laser with wavelength of 532 nm was employed to estimate the crystalline size of 66 nm TiO_2 films. J.A. Woollam's spectroscopic ellipsometry (J.A. Woollam Co., Lincoln, NE, USA) was used to study the optical properties and homogeneity of TiO_2 films along the growth direction. To study the silicon surface passivation, the effective minority carrier lifetimes were obtained by Sinton's WCT-120 (Sinton Instruments, Boulder, CO, USA) in quasi-steady-state photo-conductance (QSSPC) mode with a light bias for high resistivity Si wafers [29,30].

For the passivating-contact applications of c-Si solar cells, we go further to discuss the reflectivity and Si surface passivation of TiO_2/SiN_x stacks composed of 8-nm-thick TiO_2 and 72-nm-thick SiN_x. The capping layers, i.e., SiN_x film, were grown by plasma-enhanced chemical vapor deposition (PECVD) with reactant gases of SiH_4 (25 sccm) and NH_3 (25 sccm) at substrate temperature of 200 °C, under pressure of 0.65 torr, and radio frequency power of 90 watt. Reflectivity of samples ranging from the wavelength of 300 nm to 1200 nm was measured by Hitachi U-4100 (Hitachi, Tokyo, Japan).

3. Results

3.1. Characterization of ALD TiO_2 Thin Films

The cross-section TEM images and selective-area diffraction (SAD) patterns of TiO_2 films are shown in Figure 1. From the TEM images, we can measure the thickness of 1000-cycle TiO_2 film as 66 nm, and estimate the thicknesses of 125-cycle, 250-cycle and 530-cycle TiO_2 films as 8 nm, 15 nm and 35 nm, respectively. Amorphous TiO_2 exists in 8-nm-, 15-nm- and 35-nm-thick TiO_2 films as shown in Figure 1a–c, respectively. Anatase and amorphous TiO_2 phases coexist in the 66-nm-thick TiO_2 film as shown in Figure 1d. Anatase TiO_2 can be found near the interface of the Si and TiO_2 film. These observations can be confirmed by the SAD pattern. In Figure 1e, the SAD pattern of 35-nm-thick film is constituted by the Debye rings of a-TiO_2 and the pattern of the Si crystal. From the SAD pattern of 66-nm-thick TiO_2 shown in Figure 1f, we can find the mixture of the diffraction patterns of anatase TiO_2 and the Si crystal. According to the TEM results, we observe the phase transformation of the TiO_2 thin film as the cycle number increases during the ALD process. Heterogeneous nucleation and growth of anatase TiO_2 took place from the surface of the Si [31]. The phase transformation of the TiO_2 films from amorphous to anatase might reduce the filed-effect passivation of TiO_2 film (discuss in Section 3.2) [26,32].

Figure 2 shows the depth profile analysis of oxygen, silicon and hydrogen elements for 66-nm-thick TiO_2 films on silicon. At the interface of Si and TiO_2, we can find the large amount of hydrogen atoms which serve in the chemical surface passivation for Si. The concentration of hydrogen decreases from the interface to the surface of the TiO_2 film.

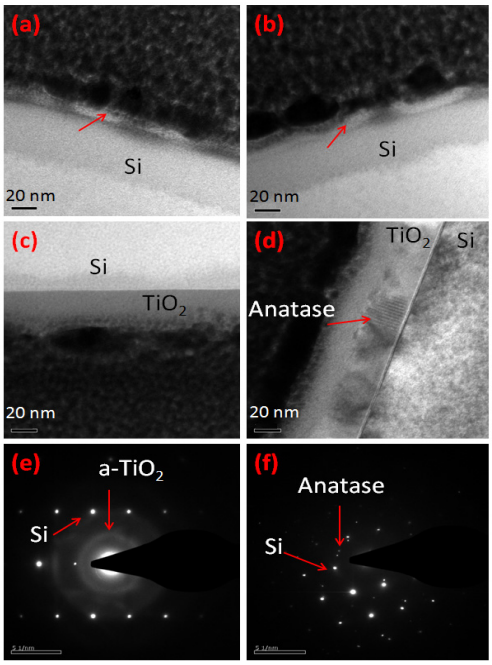

Figure 1. TEM (transmission electron microscopy) bright field images and selective-area diffraction patterns: (**a**) Bright field image of 125-cycle TiO_2 film (8 nm); (**b**) Bright field image of 250-cycle TiO_2 film (15 nm); (**c**) Bright field image of 530-cycle TiO_2 film (35 nm); (**d**) Bright field image of 1000-cycle TiO_2 (66 nm); (**e**) SAD pattern of 530-cycle TiO_2 and Si; and (**f**) SAD pattern of 1000-cycle TiO_2 and Si.

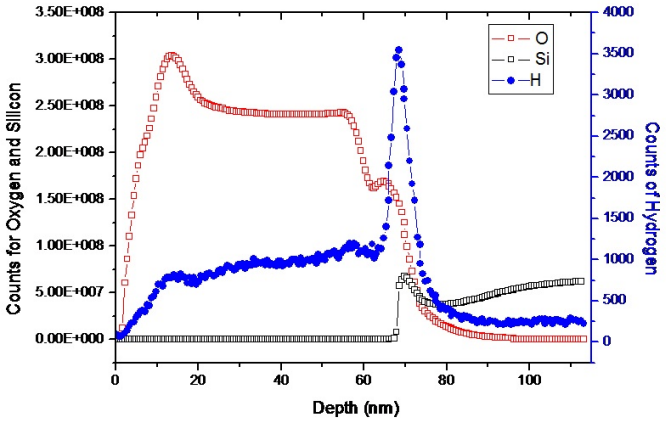

Figure 2. SIMS (secondary ion mass spectrometry) depth profiles of oxygen, silicon and hydrogen.

To further check its crystallinity, the 66-nm-thick TiO_2 film was analyzed by Raman spectroscopy. Figure 3 shows the Raman spectra of the 66-nm-thick TiO_2 film and a Si wafer. Both spectra were normalized to their maximum values of intensity (at ~520 cm^{-1} which is the phonon peak of crystalline Si). The TiO_2 film shows three relatively stronger phonon peaks located at around 141 cm^{-1}, 395 cm^{-1} and 636 cm^{-1}, and one relatively weaker phonon peak at around 195 cm^{-1} (see the inset of Figure 2). According to the report [33], these peaks can be assigned to the active phonon modes of anatase TiO_2, namely $3E_g$ (144, 196, and 638 cm^{-1}), $2B_{1g}$ (398 and 519 cm^{-1}), and $1A_{1g}$ (513 cm^{-1}). Two phonon modes at 513 and 519 cm^{-1} are not seen in the measured Raman spectrum of TiO_2, probably because of the much stronger signal of the Si phonon located at ~520 cm^{-1}. Based on the Raman results, we again confirm that the 66-nm-thick TiO_2 film contains the anatase phase.

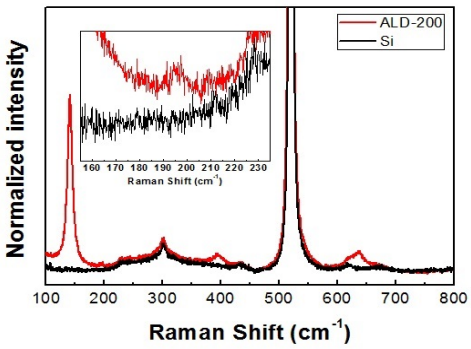

Figure 3. Raman spectra of 66-nm-thick TiO_2 film and a Si wafer. The inset shows a zoom-in around the wavenumber of 200 cm^{-1}.

When the crystalline size is smaller than the critical size, the full width at half maximum (FWHM) values of the Raman peaks become broader due to the quantum confinement effect. Therefore, we can deduce the crystalline size from the Raman results. The FWHM of the 144 cm^{-1} peak is about 10 cm^{-1}. According to the results from other groups [33,34], the crystalline size of anatase TiO_2 embedded in 66-nm-thick film should be larger than the critical size (~20 nm). This estimation is also consistent with our TEM result shown in Figure 1d.

The 66-nm-thick TiO_2 film was also analyzed by spectroscopic ellipsometry. The software CompleteEASE (Version 4.48, J.A. Woollam Co., Lincoln, NE, USA, 1999–2010) was used to fit the experimental data. To extract the optical constants of deposited TiO_2 film, we tried to use one, two, and three optical dielectric layers to model this single deposited layer. To simplify our fitting, the Cauchy function provided by CompleteEASE was used for the optical dielectric layers. For the fitting of optical dielectric layers, the parameters of the Cauchy function (A, B, and C) and the thickness are allowed to fit. Initially, the parameter of k amplitude, which is related to the strength of the extinction coefficient, was fixed at zero in consideration of the bandgap of TiO_2. Then, in order to improve the fitting (further minimizing the mean square errors (MSE) value), the k parameter of the upper layer was allowed to fit. The obtained MSEs for the one-, two-, and three-layer models are 8.26, 2.64, and 2.48, respectively. By comparing it with the MSE value of the two-layer model, the three-layer model only improved a little, which indicates that the two-layer model is enough. Among the different fitting models, we can find the best one as shown in the inset of Figure 4. The fitting results were composed of a surface roughness layer (5.8 nm), an upper layer (20.4 nm), a lower layer (50.3 nm), and a Si substrate. Adding more layers in the model does not improve the fitting results. The thickness of the surface roughness (5.8 nm) is close to the atomic force microscopy results of the 66 nm film (4.01 nm) [32]. The total thickness (upper and lower layer) of TiO_2 around 70 nm is consistent with our estimation of 66 nm based on the growth rate of our ALD system. Moreover, the two-layer model of the TiO_2 film and its individual thickness agree with the TEM result in Figure 1d. From the TEM image, the darker region from the top of the TiO_2 layer is related to the upper layer of the ellipsometry model.

Since most of the measured spectral range is below the bandgap of TiO_2, the optical dispersion of the upper and lower layers is fitted by the Cauchy dispersion functions. The extracted indices of the refraction (n) and the extinction coefficient (k) of the upper and lower layers as functions of wavelength are shown in Figure 4. The refractive index of the lower layer closes to the refractive index of the anatase TiO_2 [35]. The upper layer shows a lower value of the refractive index and a larger value of the extinction coefficient because of its amorphous phase.

Besides, this double-layer structure is better for light harvesting than the one-layer structure [36]. To show this concept, we calculated the reflectance values for one layer of 70.7-nm-thick TiO_2 (with n and k values of the lower layer) and the two-layer TiO_2 composed of an upper layer (20.4 nm) and a lower layer (50.3 nm) on top of a planar Si wafer. By loading our extracted values of n and k and using OPAL 2, an optical calculator hosted on the PV Lighthouse website [37], the average reflectance

values for the spectral range of 380–890 nm, which is the measured spectral range of ellipsometry, are 13.8% and 11.2% for the one-layer and two-layer TiO_2, respectively.

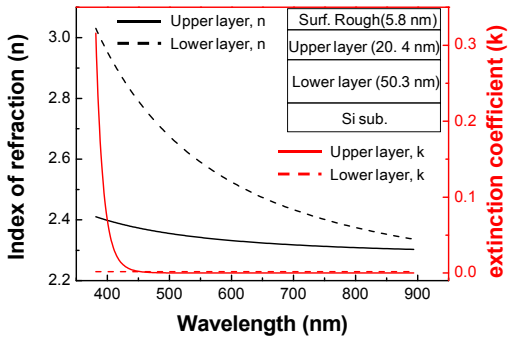

Figure 4. The extracted index of refraction (*n*) and extinction coefficient (*k*) of upper and lower layers as functions of wavelength (the inset shows the fitting model).

3.2. Silicon Surface Passivation of ALD TiO_2

Figure 5 shows the effective minority carrier lifetime as a function of the carrier density for 8-nm-thick TiO_2 film on Si. Its minority carrier lifetime value is 921 µs at a carrier density of 1.0×10^{15} cm^{-3} which was extracted using the quasi-steady-state photo-conductance (QSSPC) mode with a light bias of 0.1 suns. The result shows that the Si wafer is effectively passivated by the 8-nm-thick TiO_2 film deposited at a temperature of 200 °C. The effective lifetime (τ_eff) is a combination of the bulk lifetime (τ_bulk) and the surface lifetime (τ_sur) described as follows [38]:

$$\frac{1}{\tau\_eff} = \frac{1}{\tau\_bulk} + \frac{1}{\tau\_sur}, \quad \frac{1}{\tau\_sur} = \frac{2S}{W} \tag{1}$$

where W is the sample thickness, and S is the surface recombination velocity. Since the FZ Si wafer has a long bulk lifetime, the measured effective lifetime can be approximated to the surface lifetime. Consequently, a low surface recombination velocity of 14.93 cm/s for 8-nm-thick TiO_2 films on Si wafers is deduced.

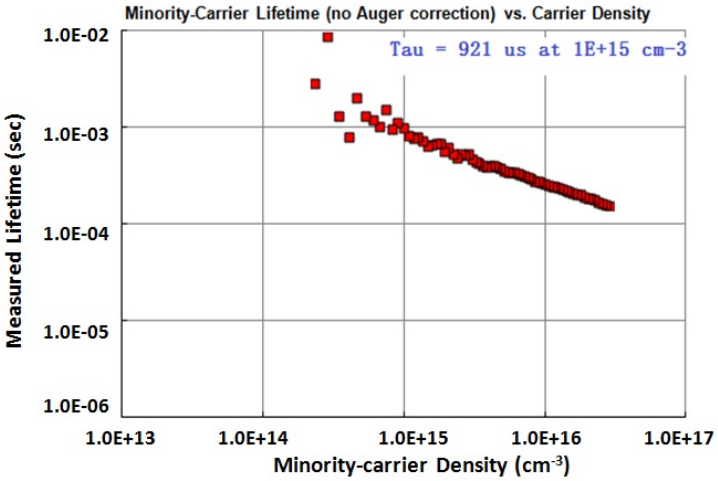

Figure 5. Minority carrier lifetime as function of carrier density for 8-nm-thick TiO_2 film deposited at substrate temperature 200 °C.

The effective minority carrier lifetimes of the other three samples with different thicknesses of TiO_2 (i.e., 15 nm, 35 nm, and 66 nm) were also investigated according to the procedures of 8-nm-thick TiO_2

films. The effective lifetimes of four samples at the injection level of 1.0×10^{15} cm^{-3} are summarized in Figure 6. The effective lifetime decreases dramatically from 921 μs for the 8-nm-thick TiO_2 film to 32 μs for the 66-nm-thick TiO_2 film. The results show that the Si surface passivation of TiO_2 films by ALD at a substrate temperature 200 °C declines as the cycle number increases. Thin TiO_2 films in amorphous phase can provide better Si surface passivation in the mechanisms of field-effect passivation and chemical passivation. The degradation of the surface passivation quality with increasing the TiO_2 thickness could be caused by stress effects and phase transformation, which has been reported and proved [26,27,32]. Phase transformation of TiO_2 at the interface could change the band structure and the interface trap density to decrease the field-effect passivation. Capacitance-voltage measurements of these films could be possible to study fixed charges and the interface trap density of TiO_2 films.

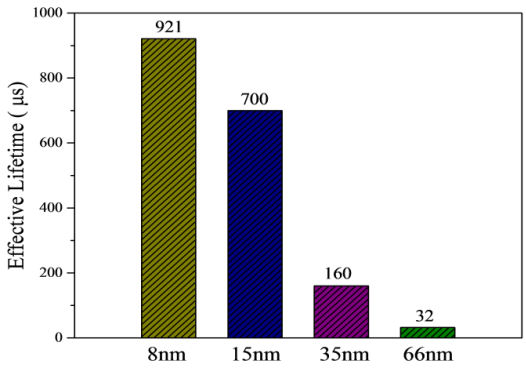

Figure 6. Minority carrier lifetime at injection level 1×10^{15} cm^{-3} for different thicknesses of ALD TiO_2 thin films deposited at 200 °C: 8 nm, 15 nm, 35 nm, and 66 nm.

Besides, atomic hydrogen, which terminates the dangling bonds of Si for chemical passivation, plays an important role in silicon surface passivation [39]. From the results of SIMS in Figure 2, we can find that atomic hydrogen accumulates at the interface of Si and TiO_2 films. We proposed that it might be another reason that ultrathin TiO_2 films have a better performance of surface passivation. The TiO_2 films with a lower thermal budget during the deposition and in the amorphous phase could keep more hydrogen atoms at the interface of the Si and TiO_2. Therefore, as the thickness of the TiO_2 thin films increases during ALD growth, stress effects, phase transformation of TiO_2 films, atomic hydrogen and a greater thermal budget from the chamber could be reasons to decrease the silicon surface passivation of TiO_2 films.

Forming gas annealing (FGA) of TiO_2 films was a strategy to enhance chemical surface passivation by the diffusion of atomic hydrogen. However, FGA at high temperatures will degrade the field-effect passivation of TiO_2 films due to the phase transformation from amorphous to anatase [26]. In order to study the thermal budget effect on the silicon surface passivation of TiO_2 films, one sample was deposited for 250 cycles without post-deposition annealing, and another was deposited for 250 cycles with post-deposition annealing at 200 °C for more 6000 s in the chamber. The effective minority carrier lifetime as a function of the carrier density is shown in Figure 7, and the sample with post-deposition annealing has a lower effective lifetime. The thermal budget from the chamber is obviously another reason to cause the decrease of silicon surface passivation. This could be because the thermal effect could cause the atomic hydrogen to diffuse out of the interface of Si and TiO_2 and decrease the chemical passivation.

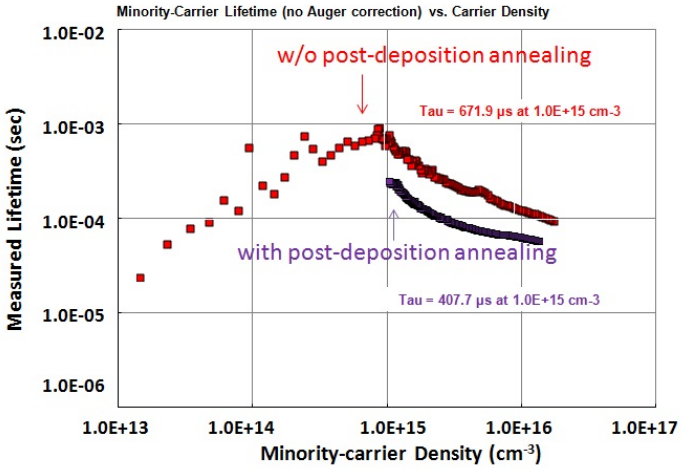

Figure 7. Minority carrier lifetime as function of carrier density for two TiO_2 films: One is deposited for 250 cycles without post-deposition annealing, and another is deposited for 250 cycles with post-deposition annealing at 200 °C for more 6000 s in the chamber.

3.3. Reflectivity and Surface Passivation of TiO_2/SiN_x Stacks

Figure 8 shows the reflectivity as a function of wavelengths from 300 nm to 1200 nm for Si wafer; 8-nm-thick, 15-nm-thick, 35-nm-thick, and 66-nm-thick TiO_2 films; and TiO_2/SiN_x stacks on Si. For samples with TiO_2 films deposited on the Si wafers, their reflectivity decreases as the thickness of the TiO_2 films increases. According to the theory of quarter-wavelength anti-reflection coating ($d = \lambda/4n_{TiO_2}$, d is the thickness and n_{TiO_2} is the refractive index of TiO_2), the (first-order) wavelength at minimum reflection red-shifts as the film thickness increases. As the wavelength at minimum reflection for the thicker TiO_2 films on Si shifts closer to the wavelength of the peak intensity of the solar spectrum for the thicker TiO_2 films on Si, they can have a better ability to harvest light. The results show that the 66-nm-thick TiO_2 film can be a good anti-reflection coating layer for Si solar cells. However, the phase transformation and post-deposition annealing could cause the surface passivation of 66-nm-thick TiO_2 film to decline.

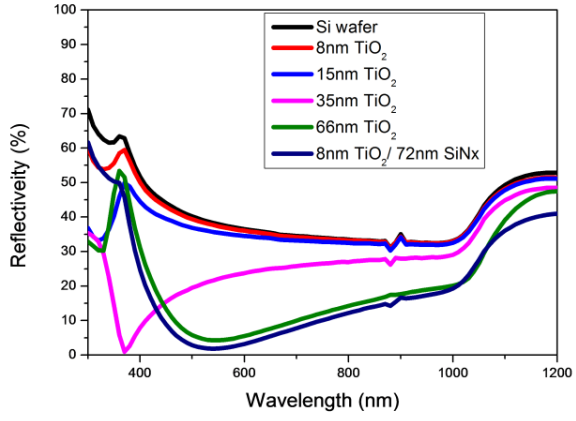

Figure 8. Reflectivity of Si wafer, Si with different thicknesses TiO_2 layers and TiO_2/SiN_x stacks as function of wavelengths from 300 nm to 1200 nm.

In this paragraph, we go further to study the optical properties and surface passivation of TiO_2/SiN_x stacks on Si for future applications on the front side of *p*-type c-Si solar cells. TiO_2/SiN_x stacks are composed of an 8-nm-thick TiO_2 film deposited by ALD and a 72-nm-thick SiN_x film deposited by plasma-enhanced chemical vapor deposition (PECVD). From the measured reflectivity

shown in Figure 8, TiO_2/SiN_x stacks have reflectivity as low as 66-nm-thick TiO_2 films which can serve as an anti-reflection coating layer for Si solar cells.

SiN_x thin film deposited by PECVD not only is the mainstream option for anti-reflection coatings in c-Si solar cells, but it also serves as the passivation layer due to the atomic hydrogen in the film. During the process of solar cells, hydrogen atoms can diffuse and serve in the chemical passivation [40]. For the silicon surface passivation of TiO_2/SiN_x stacks, Figure 9 shows the effective carrier lifetimes of bare Si wafer, TiO_2/SiN_x stacks, 80-nm-thick SiN_x films deposited by PECVD, and 66-nm-thick TiO_2 films deposited by ALD on Si at the injection level of 1.0×10^{15} cm^{-3}. The error bar of the effective carrier lifetime is the standard deviation of six samples for individual conditions. Some degree of silicon surface passivation by TiO_2/SiN_x stacks can be found, and the stacks have a better performance of surface passivation than that of SiN_x and TiO_2 layers. TiO_2/SiN_x stacks have excellent optical properties and effective Si surface passivation so they can be a potential material for c-Si solar cells. Compared with 8-nm-thick TiO_2 film, the effective lifetime decreases after the capping layer of SiN_x. The reason might be similar to that for 66-nm-thick TiO_2 film. Stress effects, phase transformation of TiO_2 films and the thermal budget effect induced by the PECVD process make the performance of the surface passivation decrease. For further applications on c-Si solar cells, lower-temperature deposition of the SiN_x capping layer and forming gas annealing of TiO_2/SiN_x stacks might be better.

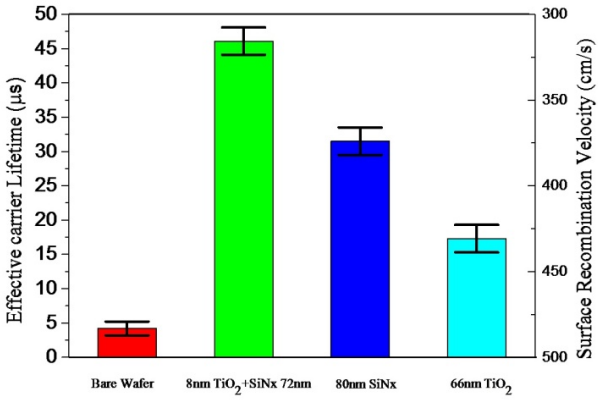

Figure 9. The average effective lifetime at the injection level 1×10^{15} cm^{-3} for bare Si wafers, TiO_2/SiN_x stacks, 80-nm-thick SiN_x films by PECVD, and 66-nm-thick TiO_2 films by ALD.

4. Discussion

TiO_2 thin films with different thicknesses were grown by ALD at a temperature of 200 °C for silicon surface passivation, anti-reflection coatings and passivating contact. From the characterization of 66-nm-thick TiO_2 thin films by TEM, SIMS, Raman spectroscopy, and ellipsometry, we observed the phase formation of anatase TiO_2 distributing non-homogeneously along the growth direction, deduced its crystal size, completed a depth profile analysis of atomic hydrogen and investigated the optical properties. Amorphous TiO_2 thin films grown by ALD at a temperature of 200 °C have a good performance in silicon surface passivation. The surface recombination velocity of 8-nm-thick TiO_2 films can reach 14.93 cm/s at the injection level of 1×10^{15} cm^{-3}. However, the Si surface passivation of TiO_2 film strongly depends on its thickness (8 nm, 15 nm, 35 nm and 66 nm), which is associated with stress effects and atomic hydrogen relating to the phase transformation and thermal stability of TiO_2 films. For further applications on the passivating contact of c-Si solar cells, we also studied the performance of anti-reflection and Si surface passivation for a stack composed of an 8-nm-thick TiO_2 film deposited by ALD and a capping layer of 72-nm-thick SiN_x deposited by PECVD. Low reflectivity and some degree of surface passivation were observed when using TiO_2/SiN_x stacks on Si wafers.

Acknowledgments: The authors acknowledge the Ministry of Science and Technology R.O.C. (MOST 104-2221-E-218-002, 104-2221-E-259-001 and 104-2221-E-009-167) for financially supporting this study. Thanks to the R&D department of E-Ton Solar Tech. Co. LTD for the measurements of the WCT-120 and Hitachi U-4100.

Author Contributions: I.-S.Y. and H.-E.C. conceived and designed the experiments; I-H.C. performed the experiments; I.-S.Y. and Z.-P.Y. analyzed the data and wrote the paper.

Conflicts of Interest: The authors declare no conflict of interest.

References

1. Green, M.A. The path to 25% silicon solar sell efficiency: History of silicon cell evolution. *Prog. Photovoltaics Res. Appl.* **2009**, *17*, 183–189. [CrossRef]
2. Aberle, A.G. Surface passivation of crystalline silicon solar cells: A review. *Prog. Photovoltaics Res. Appl.* **2000**, *8*, 473–487. [CrossRef]
3. Werner, F.; Veith, B.; Tiba, V.; Poodt, P.; Roozeboom, F.; Brendel, R.; Schmidt, J. Very low surface recombination velocities on *p*- and *n*-type c-Si by ultrafast spatial atomic layer deposition of aluminum oxide. *Appl. Phys. Lett.* **2010**, *97*, 162103. [CrossRef]
4. Ge, J.; Tang, M.; Wong, J.; Zhang, Z.; Dippell, T.; Doerr, M.; Hohn, O.; Huber, M.; Wohlfart, P.; Aberle, A.G.; et al. Excellent silicon surface passivation achieved by industrial inductively coupled plasma deposited hydrogenated intrinsic amorphous silicon suboxide. *In. J. Photoenergy* **2014**, *2014*. [CrossRef]
5. Breitenstein, L.; Richter, A.; Hermle, M.; Warta, W. Impact of wet-chemical cleaning on the passivation quality of Al_2O_3 layers. In Proceedings of the 37th IEEE Photovoltaic Specialists Conference, Seattle, WA, USA, 19–24 June 2011; pp. 1400–1404.
6. Schmidt, J.; Veith, B.; Werner, F.; Zielke, D.; Brendel, R. Silicon surface passivation by ultrathin Al_2O_3 films and Al_2O_3/SiN*x* stacks. In Proceedings of the 35th IEEE Photovoltaic Specialists Conference, Honolulu, HI, USA, 20–25 June 2010; pp. 885–890.
7. Hoex, B.; Schmidt, J.; Pohl, P.; Van de Sanden, M.C.M.; Kessels, W.M.M. Silicon surface passivation by atomic layer deposited Al_2O_3. *J. Appl. Phys.* **2008**, *104*. [CrossRef]
8. Vermang, B.; Werner, F.; Stals, W.; Lorenz, A.; Rothschild, A.; John, J.; Poortmans, J.; Mertens, R.; Gortzen, R.; Poodt, P.; et al. Spatially-separated atomic layer deposition of Al_2O_3, a new option for high-throughput Si solar cell passivation. *Prog. Photovoltaics Res. Appl.* **2010**, *19*, 733–739. [CrossRef]
9. Lee, B.G.; Li, S.; Von Gastrow, G.; Yli-Koski, M.; Savin, H.; Malinen, V.; Skarp, J.; Choi, S.; Branz, H.M. Excellent passivation and low reflectivity with atomic layer deposited bilayer coatings for *n*-type silicon solar cells. *Thin Solid Films* **2014**, *550*, 541–544. [CrossRef]
10. Davis, K.O.; Jiang, K.; Habermann, D.; Schoenfeld, W.V. Tailoring the optical properties of APCVD titanium oxide films for all-oxide multi-layer anti-reflection coatings. *IEEE J. Photovoltaics* **2015**, *5*, 1265–1270. [CrossRef]
11. Suh, D. Stacked and nanolaminated Al_2O_3/TiO_2 for surface passivation and encapsulation of silicon. *Phys. Status Solidi (RRL)* **2015**, *9*, 344–347. [CrossRef]
12. Benner, F.; Jordan, P.M.; Richter, C.; Simon, D.K.; Dirnstorfer, I.; Knaut, M.; Bartha, J.W.; Mikolajick, T. Atomic layer deposited high-κ nanolaminates for silicon surface passivation. *J. Vac. Sci. Technol. B* **2014**, *32*. [CrossRef]
13. Dirnstorfer, I.; Chohan, T.; Jordan, P.M.; Knaut, M.; Simon, D.K.; Bartha, J.W.; Mikolajick, T. Al_2O_3-TiO_2 nanolaminates for conductive silicon surface passivation. *IEEE J. Photovoltaics* **2016**, *6*, 86–91. [CrossRef]
14. Melskens, J.; Van de Loo, B.W.H.; Macco, B.; Vos, M.F.J.; Palmans, J.; Smit, S.; Kessels, W.M.M. Concepts and prospects of passivating contacts for crystalline silicon solar cells. In Proceedings of the 42nd IEEE Photovoltaic Specialists Conference, New Orleans, LA, USA, 14–19 June 2015; pp. 1–6.
15. Richards, B.S. Comparison of TiO_2 and other dielectric coatings for buried contact solar cells: A review. *Prog. Photovoltaics Res. Appl.* **2004**, *12*, 253–281. [CrossRef]
16. Lee, Y.-T.; Lin, F.-R.; Lin, T.C.; Chen, C.-H.; Pei, Z. Low-temperature, chemically grown titanium oxide thin films with a high hole tunneling rate for Si solar cells. *Energies* **2016**, *9*. [CrossRef]
17. Rohatgi, A.; Doshi, P.; Moschner, J.; Lauinger, T.; Aberle, A.G.; Ruby, D.S. Compressive study of rapid low-cost silicon surface passivation technologies. *IEEE Tran. Electron Devices* **2000**, *47*, 987–993. [CrossRef]
18. Doeswijk, L.M.; De Moor, H.H.C.; Blank, D.H.A.; Rogalla, H. Passivating TiO_2 coatings for silicon solar cells by pulsed laser deposition. *Appl. Phys. A* **1999**, *69*. [CrossRef]

19. Thomson, A.F.; Lynn, S.Z.; McIntosh, K.R. Passivation of silicon by negatively charged TiO_2. In Proceedings of the 25th EUPVSEC, Valencia, Spain, 6–10 September 2010; pp. 1146–1153.
20. Thomson, A.F.; McIntosh, K.R. Light-enhanced surface passivation of TiO_2-coated silicon. *Prog. Photovoltaics Res. Appl.* **2012**, *20*, 343–349. [CrossRef]
21. Yu, I.-S.; Wang, Y.-W.; Cheng, H.-E.; Yang, Z.-P.; Lin, C.-T. Surface passivation and antireflection behavior of ALD TiO_2 on *n*-type silicon for solar cells. *Int. J. Photoenergy* **2013**, *2013*. [CrossRef]
22. Liao, B.; Hoex, B.; Aberle, A.G.; Chi, D.; Bhatia, C.S. Excellent c-Si surface passivation by low-temperature atomic layer deposited titanium oxide. *Appl. Phys. Lett.* **2014**, *104*. [CrossRef]
23. Liao, B.; Hoex, B.; Shetty, K.D.; Basu, P.K.; Bhatia, C.B. Passivation of boron-doped industrial silicon emitters by thermal atomic layer deposited titanium oxide. *IEEE J. Photovoltaics* **2015**, *5*, 1062–1065. [CrossRef]
24. Avasthi, S.; McClain, W.E.; Mam, G.; Kahn, A.; Schwartz, J.; Sturm, J.C. Hole-blocking titanium-oxide/silicon heterojunction and its application to photovoltaics. *Appl. Phys. Lett.* **2013**, *102*. [CrossRef]
25. Yang, X.; Zheng, P.; Bi, Q.; Weber, K. Silicon heterojunction solar cells with electron selective TiO_x contact. *Sol. Energy Mater. Sol. Cells* **2016**, *150*, 32–38. [CrossRef]
26. Yang, X.; Bi, Q.; Ali, H.; Davis, K.O.; Schoenfeld, W.V.; Weber, K. High performance TiO_2-based electron-selective contacts for crystalline silicon solar cells. *Adv. Mater.* **2016**, *28*, 5891–5897. [CrossRef] [PubMed]
27. Gad, K.M.; Vossing, D.; Rimin, A.; Rayner, B.; Reindl, L.M.; Mohney, S.E.; Kasemann, M. Ultrathin titanium dioxide nanolayers by atomic layer deposition for surface passivation of crystalline silicon. *IEEE J. Photovoltaics* **2016**, *6*, 649–653. [CrossRef]
28. Cheng, H.-E.; Chen, C.-C. Morphological and photoelectrochemical properties of ALD TiO_2 films. *J. Electrochem. Soc.* **2008**, *155*, D604–D607. [CrossRef]
29. McIntosh, K.R.; Guo, J.-H.; Abbott, M.D.; Bardos, R.A. Calibration of the WCT-100 photoconductance instrument at low conductance. *Prog. Photovoltaics Rese. Appl.* **2008**, *16*, 279–287. [CrossRef]
30. Sinton, R.A.; Cuevas, A.; Stuckings, M. Quasi-steady-state photoconductance: A new method for solar cell material and device characterization. In Proceedings of the 25th IEEE Photovoltaic Specialists Conference, Washington, DC, USA, 13–17 May 1996; pp. 457–460.
31. Won, D.-J.; Wang, C.-H.; Jang, H.-K.; Choi, D.-J. Effect of thermally induced anatase-to-rutile phase transition in MOCVD growth TiO_2 films on structural and optical properties. *Appl. Phys. A* **2001**, *73*, 595–600. [CrossRef]
32. Yu, I.-S.; Chang, I.-H.; Cheng, H.-E.; Lin, Y.-S. Surface passivation of c-Si by atomic layer deposition TiO_2 thin films deposited at low temperature. In Proceedings of the 40th IEEE Photovoltaic Specialists Conference, Denver, CO, USA, 8–13 June 2014; pp. 1271–1274.
33. Georgescu, D.; Baia, L.; Ersen, O.; Baia, M.; Simon, S. Experimental assessment of phonon confinement in TiO_2 anatase nanocrystallites by Raman spectroscopy. *J. Raman Spectrosc.* **2012**, *43*, 876–883. [CrossRef]
34. Sahoo, S.; Arora, A.K.; Sridharan, V. Raman line shapes of optical phonons of different symmetries in anatase TiO_2 nanocrystals. *J. Phys. Chem. C* **2009**, *113*, 16927–16933. [CrossRef]
35. Jellison, G.E.; Boatner, L.A., Jr.; Budai, J.D.; Jeong, B.-S.; Norton, D.P. Spectroscopic ellipsometry of thin film and bulk anatase (TiO_2). *J. Appl. Phys.* **2003**, *93*, 9537–9541. [CrossRef]
36. Richards, B.S. Single-material TiO_2 double-layer antireflection coatings. *Sol. Energy Mater. Sol. Cells* **2003**, *79*, 369–390. [CrossRef]
37. PV Lighthouse. Available online: http://www.pvlighthouse.com.au/calculators/OPAL%202/OPAL%202.aspx (accessed on 20 May 2015).
38. Kane, D.E.; Swanson, R.M. Measurement of the emitter saturation current by a contactless photoconductivity decay method. In Proceedings of the 18th IEEE Photovoltaic Specialists Conference, Las Vegas, NV, USA, 21–25 October 1985; pp. 578–583.
39. Rahman, M.Z.; Khan, S.I. Advances in surface passivation of c-Si solar cells. *Mater. Renew. Sustain. Energy* **2012**, *1*. [CrossRef]
40. Wan, Y.; McIntosh, K.R.; Thomson, A.F. Characterisation and optimization of PECVD SiN_x as an antireflection coating and passivation layer for silicon cells. *AIP Adv.* **2013**, *3*. [CrossRef]